Thermal stability of two-dimensional gold nanocrystal superlattices

2009 J. Phys.: Condens. Matter 21 264011

(http://iopscience.iop.org/0953-8984/21/26/264011)

IOP Publishing Journal of Physics: Condensed Matter

J. Phys.: Condens. Matter **21** (2009) 264011 (6pp) doi:10.1088/0953-8984/21/26/264011

Thermal stability of two-dimensional gold nanocrystal superlattices

István Robel[1], Xiao-Min Lin[1], Michael Sprung[2] and Jin Wang[2]

[1] Center for Nanoscale Materials, Argonne National Laboratory, Argonne, IL 60439, USA
[2] X-ray Science Division, Argonne National Laboratory, Argonne, IL 60439, USA

Received 10 December 2008
Published 11 June 2009
Online at stacks.iop.org/JPhysCM/21/264011

Abstract

The thermal stability of highly ordered two-dimensional superlattices consisting of dodecanethiol-ligated Au nanoparticles has been investigated using *in situ* grazing incidence small-angle x-ray scattering in air and in vacuum. In the lower temperature region (<70 °C), annealing in air results in a minimal change of superlattice structure, whereas annealing in vacuum leads to a considerable lattice contraction and a decrease in long-range order. At higher temperatures (>100 °C), ligand desorption causes nanocrystals to sinter locally, destroying quasi-long-range order. The sintering process is significantly enhanced in vacuum compared to the case in air due to the increased desorption rate of thiol ligands under low pressure.

(Some figures in this article are in colour only in the electronic version)

1. Introduction

Colloidal nanocrystals of semiconductors, noble metals, and transition metals have been the focus of intense research during the past two decades, largely driven by their unique electronic, optical, and magnetic properties [1–4]. The prospect of using nanocrystals as building blocks to form superlattices and to create macroscopic functional devices has generated significant interest in understanding nanoscale self-assembly [5–9]. Combining nanocrystals with different sizes [10], compositions [6] and even shapes [11] could lead to new materials with fascinating collective properties. However, before self-assembled nanocrystal superlattices can be considered for applications such as sensors [12], electronic devices [7] or magnetic storage media [13], their thermal stability needs to be further investigated. Indeed, nanoscale materials show significantly lower melting temperatures compared to their bulk counterparts [14], and the organic ligands that stabilize a nanocrystal superlattice can undergo melting transition at room temperature or even below [15–17].

A few existing experiments illustrate a complex picture when the nanoparticle arrays are thermally annealed. Korgel used small-angle x-ray scattering (SAXS) to study three-dimensional (3D) superlattices of silver nanocrystals coated with alkanethiols of different lengths [18]. He observed a narrow temperature range in which the disordering of the nanocrystal superlattice resembles the melting of an atomic solid, whereas above this 'melting' point and within a certain temperature range, a bicontinuous phase with long-range spatial correlation exists. This phase was attributed to thermal fluctuation of displaced ligand chains. Sandhyarani *et al* studied 3D superlattices of octadecanethiol- and octanethiol-protected small silver clusters using differential scanning calorimetry and x-ray diffraction [19]. They reported a reversible melting and crystallization transition when the temperature was cycled through the melting point of the thiol ligand. On the other hand, a recent grazing-incidence small-angle x-ray scattering (GISAXS) study by our group on 3D dodecanethiol-ligated Au nanocrystals has revealed a irreversible continuous disordering and shrinking of the lattice parameter upon annealing [20]. In this work, we extend our study on the thermal stability of 3D Au nanocrystal superlattices to two-dimensional (2D) superlattices. GISAXS is a powerful *in situ* x-ray technique that combines the accessible length scales of SAXS and the surface sensitivity of grazing incidence, thus allowing us to study the 2D order-to-disorder transition in detail. As the rate of ligand evaporation can also affect thermal stability, we perform our measurements both in air (atmospheric pressure) and in vacuum.

2. Experimental section

2.1. Nanocrystal synthesis

Au nanocrystals were synthesized using a digestive ripening procedure described in detail in reference [21]. Briefly, 68 mg

of gold chloride and 208 mg of didodecyldimethylammonium bromide (DDAB) were dissolved in 20 ml of toluene. 26 mg of sodium borohydride in 74 μl of water was added under vigorous stirring (30–60 min) until a wine colored solution developed. This was followed by the addition of 1.6 ml of dodecanethiol (DDT) to the reaction flask to complete the DDAB-DDT ligand exchange. 30 ml of 200 proof ethanol was then added to precipitate the as-prepared particles. After the precipitates were dried, 20 ml of toluene and 1.6 ml of DDT was added, followed by heating the solution under reflux on a hotplate for 3 h. This digestive ripening process helps to narrow the size distribution of the gold colloids, as demonstrated in several previous studies [21, 22]. After the colloid was cooled to room temperature over night, the top layer of the solution was extracted, precipitated, and washed with ethanol several times. Finally, the dried sample was dissolved in toluene to a number concentration of $\sim 10^{13}$ ml^{-1}. This procedure results in Au nanocrystal diameters in the 5.5–7.5 nm range, with average diameters determined by the initial injection of borohydride and the amount of water present in the reaction. Typical size distributions are in the 5–7% range as indicated by TEM measurements.

2.2. Self-assembly of 2D superlattices

We have previously shown that the assembly mechanism for 3D and 2D superlattices is fundamentally different: the formation of 3D nanocrystal superlattices in solution is understood to be the analog of conventional crystal growth from atoms and molecules [23], although the interaction between the nanocrystal building blocks is quite different from the interactions on the atomic scale. For noble metal nanocrystals, van der Waals interaction plays the role of the attractive force and the steric hindrance caused by the interdigitation of organic ligand molecules serves as the repulsion. On the other hand, the formation of 2D superlattices requires the confinement of nanocrystals to a 2D surface or interface, typically achieved through depositing nanocrystals directly on solid substrates [24–26] or on the liquid–air interface using a Langmuir trough [27]. Recently, it was found that 2D superlattice domains can spontaneously form and grow in size at the liquid–air interface using a simple drop drying process [28, 29]. The underlying mechanism for this unique phenomenon is the slow diffusion of nanocrystals in comparison with the faster motion of the drying liquid surface. The interaction between nanocrystals and the liquid–air interface is also enhanced by the addition of a small excess of ligand molecules to the colloidal droplet. As the droplet evaporation progresses, the density of nanocrystals at the interface increases, leading to the formation of 2D superlattices when the critical concentration for 2D crystallization is reached. The highly ordered 2D superlattice domains typically can grow to tens of microns in size and can be tracked with conventional optical microscopy [29]. Such 2D Au nanocrystal superlattices are used in our experiments upon complete drying of the droplet on a Si/SiN substrate (figure 1).

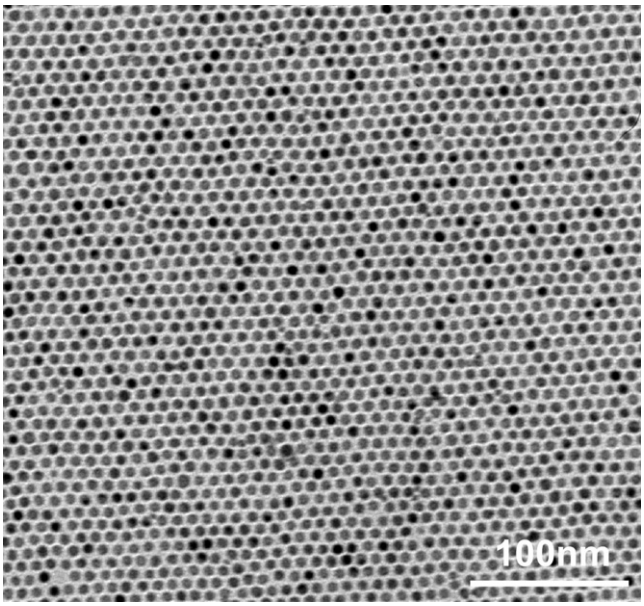

Figure 1. Transmission electron micrograph of a 2D gold nanocrystal superlattice formed by the drop drying technique on a Si/SiN nitride membrane substrate.

2.3. GISAXS setup

GISAXS measurements were carried out at the XOR 8-ID-E beamline of the Advanced Photon Source. A monochromatic x-ray energy of 7.35 keV (x-ray wavelength of 1.687 Å) selected by a single bounce Si(111) crystal with energy resolution of $\Delta E/E \sim 10^{-4}$ was used throughout the experiments. In a typical measurement, x-rays were incident on the Au nanocrystal monolayers under a fixed angle of 0.2°. The beam size was confined to 25 μm in vertical direction and 140 μm horizontally, resulting in a footprint on the sample of $\sim$4 mm long along the beam direction (spanning the entire nanocrystal monolayer sample length). GISAXS patterns were collected using a MAR165 CCD detector (79.138 μm microns pixel pitch in 2 × 2 binning mode with 2048 × 2048 pixels) at a distance of $\sim$1167 mm from the sample (figure 2(a)). This setup was able to detect a maximum horizontal scattering angle of $\sim$3.97° (or an out-of-plane scattering vector of $\sim$2.3 nm^{-1}). The samples were prepared on Si/SiN substrates and mounted on a Lakeshore 340 temperature-controlled copper heating stage. A Pt100 resistor measured the stage temperature. Due to the negligible heat capacity of the Si/SiN chips compared to the massive copper stage and assuming a good thermal contact enabled by thermal grease, we estimate that the temperature difference between the sample and heating stage is less than 1 °C. Peltier-cooling was employed to decrease the temperature of the sample. GISAXS measurements were carried out with samples in air and in a vacuum of 10^{-4}–10^{-5} Torr.

3. Results and discussions

Figure 2(b) shows a typical small angle x-ray scattering pattern obtained from a highly ordered Au nanocrystal monolayer at

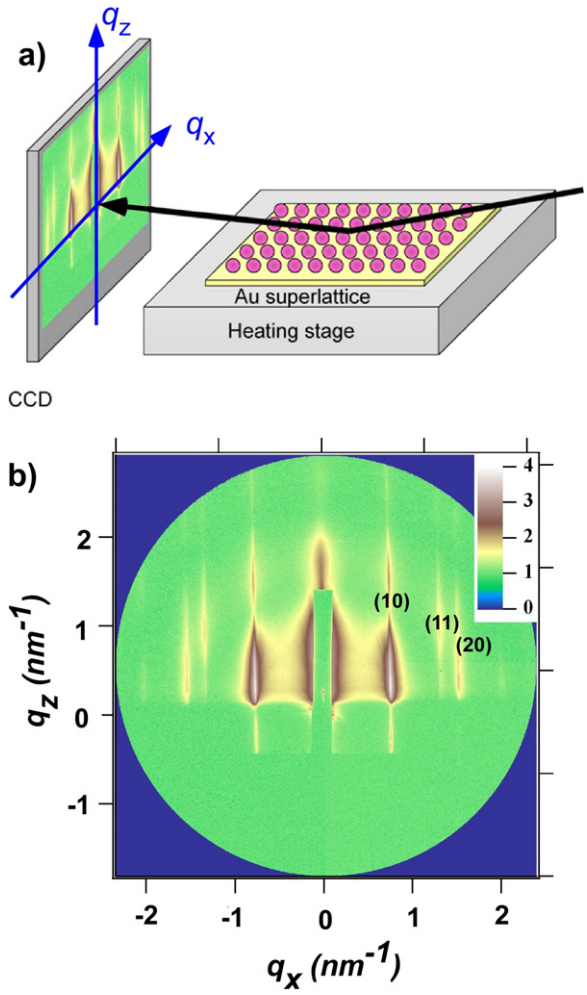

Figure 2. (a) Schematic diagram of GISAXS setup. (b) A typical scattering pattern collected on the CCD for a highly ordered 2D gold nanocrystal superlattice. (The intensity of the scattering pattern is plotted on a log scale in order to enhance the contrast.)

room temperature. The pattern consists of scattering rods (Fourier-transforms of the 2D hexagonally packed particles) that intersect the plane of the detector. Intensity variations in the q_z direction are due to the form factor of the approximately spherical Au nanocrystals and is consistent with the form factor directly measured from the colloidal solution. Multiple peaks are observed corresponding to scattering in the (10), (11) and (20) directions as indicated in the figure. A comparison of the calculated interplane spacings from (10), (11) and (20) peaks indicates a hexagonal 2D array ($d_{10}/d_{20} = 2.0$, $d_{10}/d_{11} = \sqrt{3}$), which is consistent with the TEM image shown in figure 1. The position of the peaks is determined by the lattice constant of the 2D nanocrystal array. The width of the peaks indicates the degree of ordering, which is more illustrative in the 2D linear intensity GISAXS pattern. Therefore, the structural changes of the superlattices at high temperature can be tracked by the change of these peaks. For the as-prepared samples at room temperature, we obtain an interparticle spacing of 8.3 nm, consistent with the measured particle size of 7 nm stabilized by DDT ligands. Our previous experiments have shown that excess DDT ligands play an important role in the formation of nanocrystal superlattices. Besides affecting the interfacial energy of the liquid–air interface, the excess ligands in solution also ensure a complete coating of ligand molecules on the surface of nanocrystals. Moreover, thiol ligands fill interstitial voids between particles, establishing a well-defined lattice spacing [30] and thus maintaining the long-range spatial correlation of the superlattice.

We examined the thermal stability of the 2D superlattices in two different temperature regions classified by the different thermal behavior of the ligands: the low temperature region (<70 °C) and the high temperature region (>100 °C). In the low temperature region, ligand desorption from the nanocrystal surface is not a major concern. However, the ligands on the surface of nanocrystals could undergo a first-order 'melting transition', in which the alkane chains of the ligand transform from a highly ordered state to a disordered state. This is represented by an increase in *gauche* bond conformation compared to the *trans* conformation [15]. The temperature at which the melting transition occurs depends on both the chain length as well as the curvature of the nanoparticle surface. The melting temperature of DDT ligands on the extended gold surface is 50 °C [31], whereas on a 2 nm cluster is −10–3 °C [15, 16]. For slightly larger particles (5–6 nm, close in size to what we used in our studies) the melting transition was reported to be 33 °C [17].

Figure 3 shows the evolution of the normalized (10) peak as a function of temperature when the sample is heated to 65 °C and cooled back to 30 °C, both in air and in vacuum. A comparison of these two scenarios shows a striking difference. There is little to no change in the peak position and width when the superlattice is heated in air, but in vacuum the nanocrystal array shows a irreversible shrinkage of the lattice constant and a broadening of the (10) peak, indicating an increase of lattice disorder. The change of the corresponding lattice parameter during consecutive heating and cooling cycles is shown in figure 4. A contraction of the interparticle spacing from 8.25 to 8.07 nm is observed when the superlattice is heated from 30 to 65 °C in vacuum (a change of 2%). The stress induced by this lattice contraction results in large cracks of the nanocrystal monolayer with micron size domains, easily visible in optical microscopy. These data are clearly different from the reversible superlattice phase transition induced by the melting and recrystallization of surface ligands [19].

The different behavior of the low-temperature annealing can be traced to the amount of free thiol molecules in the arrays. As we mentioned above, excess thiols play an essential role in the formation of nanocrystal arrays with the drying-droplet method. Due to the slow evaporation rate of DDT at room temperature, unbound molecules are present in the sample even after drying, forming a spacer between nanocrystals in addition to the stabilizing thiols directly bound to the Au surface. The evaporation rate of unbound thiols is greatly enhanced in vacuum, especially at elevated temperatures. During the typical time frame of the experiment with a heating rate of about 2–3 °C min^{-1} (10–15 min heating time to 65 °C), excess thiols from the interparticle space could evaporate significantly more rapidly in vacuum than in air. This

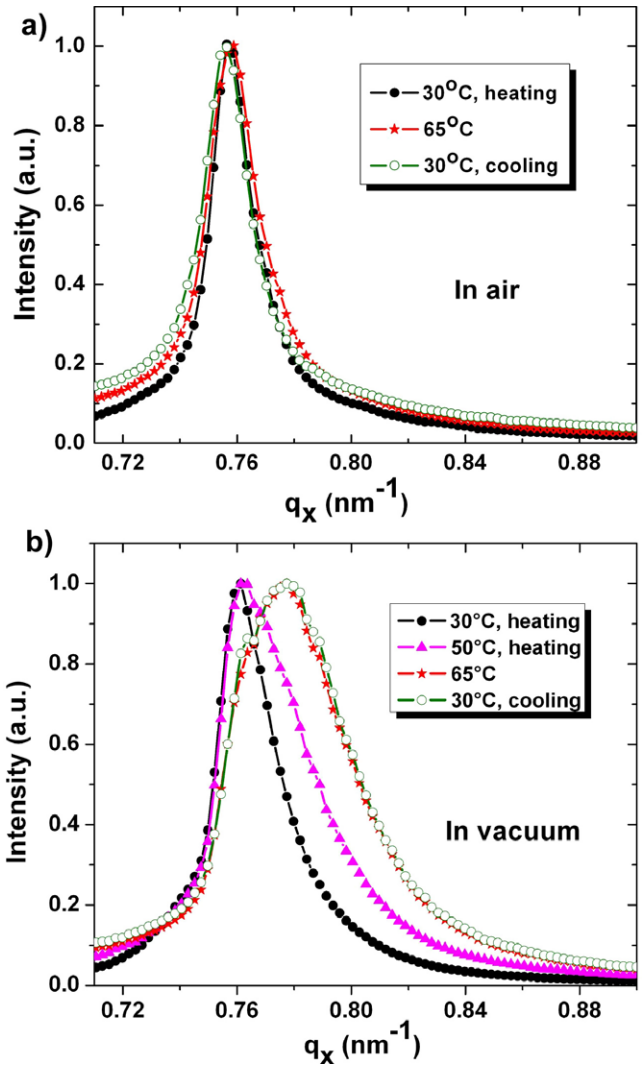

Figure 3. Change of the normalized (10) scattering peak when the sample is heated to 65 °C and cooled back to 30 °C, (a) in air and (b) in vacuum.

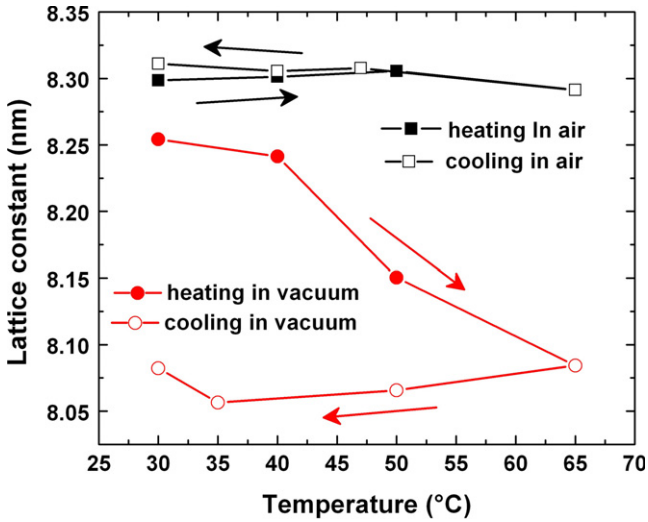

Figure 4. Change of lattice constant obtained from the shift of (10) scattering peak position when the sample is heated to 65 °C and cooled back to 30 °C both in air and in vacuum.

means that interstitial ligand density between nanoparticles in the arrays could decrease sharply in vacuum. At the same time, increasing the concentration of *gauche*-conformation ligands during a melting transition will allow more efficient ligand packing, reducing the steric repulsion between ligands and thereby resulting in a decrease of the lattice constant in the 2D array. The contraction of the superlattice after evaporation of excess thiols can be important in increasing the conductivity of nanocrystal arrays. Due to the exponential dependence of the tunneling resistivity on interparticle spacing, a 0.2 nm shrinkage of the lattice constant can give rise to several orders of magnitude increase of electric conductivity. This behavior has been reported in a Co nanocrystal array [32].

The difference in thermal stability when the sample is annealed in air and in vacuum becomes more dramatic in the high temperature region. When the sample is heated above 100 °C, the desorption of thiols attached to the Au surface becomes an important factor. Temperature-dependent scanning-tunneling microscopy measurements have shown that DDT monolayers bound to the Au (111) surface desorb at ∼125 °C [33]. Figure 5 shows the comparison of two samples that are heated to 160 °C, and then cooled back to 30 °C at a rate of 2–3 °C min^{-1}, both in air and in vacuum. The ordering of the superlattice is largely retained when the sample is heated in air, with a shift of the peak position to higher q_x values and a broadening of the peak width. On the other hand, the ordering of the superlattice heated in vacuum is completely destroyed. The large diffuse scattering near $q_x = 0$ (not shown) indicates significant sintering of particles on the surface when the sample is annealed in vacuum, resulting in a wide distribution of interparticle spacing. The most dramatic change was observed when the temperature of the sample was increased beyond 110 °C in vacuum (figure 5(e)). Although the sample in air maintains lattice order at 160 °C for short periods of time (∼a few minutes), an extended exposure to this elevated temperature over several hours leads to the gradual disintegration of the lattice order similar to that observed in vacuum at 110 °C. This confirms that the difference of thiol desorption rate between the sample heated in air and in vacuum is the main contributing factor to the different thermal stability of 2D superlattices.

4. Conclusions

We have shown that GISAXS is a powerful *in situ* technique to monitor the temperature-induced structural changes of 2D nanocrystal superlattices. Our results indicate that the thermal stability of the superlattice strongly depends on the melting transitions, the desorption rates of surface ligands and exhibits a striking difference between annealing in air and in vacuum. Therefore, for future devices that are designed based on nanocrystal superlattices, it is important to take into consideration the thermal stability of these new materials. Several approaches could be further investigated to improve the thermal stability of superlattices, such as chemical techniques

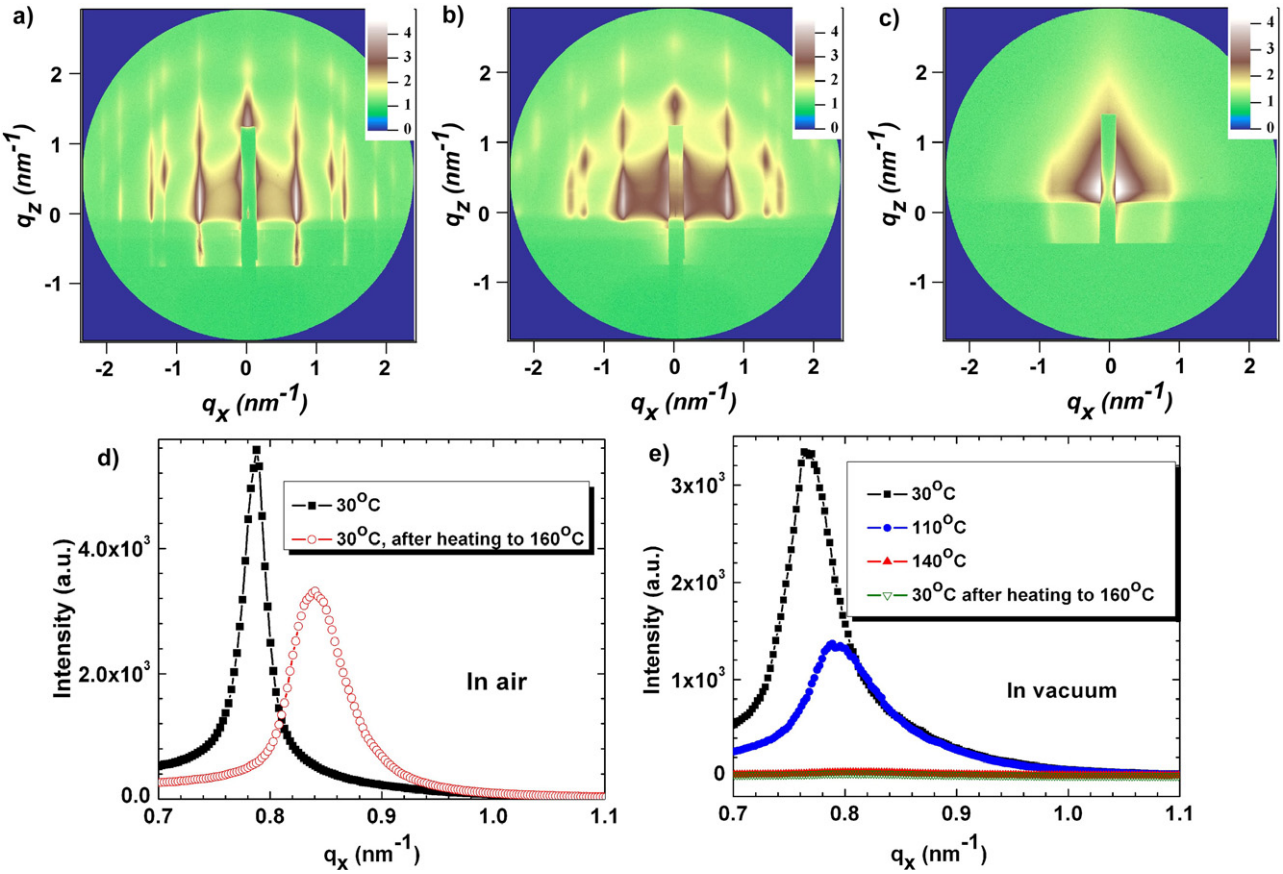

Figure 5. GISAXS patterns from a 2D gold nanocrystal superlattice (a) at 30 °C, (b) at 30 °C after being heated in air to 160 °C and cooled back to 30 °C at a rate of 2–3 °C min^{-1}, (c) at 30 °C after being heated in vacuum to 160 °C and back to 30 °C at a rate of 2–3 °C min^{-1}. Change in intensity of the (10) peak after being heated in air (d) and in vacuum (e).

based on coating the particles with a different material with higher melting temperatures, or physical techniques such as cross-linking ligands between neighboring nanocrystals by electron beam.

Acknowledgments

The use of the Advanced Photon Source and the Center for Nanoscale Materials at Argonne National Laboratory was supported by the US Department of Energy, Office of Science, Office of Basic Energy Sciences, under Contract No. DE-AC02-06CH11357.

References

[1] Talapin D V and Murray C B 2005 *Science* **310** 86–9
[2] Brust M, Walker M, Bethell D, Schiffrin D J and Kiely C 1994 *J. Chem. Soc. Chem. Commun.* 801
[3] Alivisatos A P 1996 *Science* **271** 933–7
[4] Lin X M and Samia A C S 2006 *J. Magn. Magn. Mater.* **305** 100–9
[5] Murray C B, Kagen C R and Bawendi M G 1995 *Science* **270** 1335–8
[6] Shevchenko E V, Talapin D V, Kotov N A and O'Brian S 2006 *Nature* **439** 55–9
[7] Zabet-Khosousi A and Dhirani A 2008 *Chem. Rev.* **108** 4072–124
[8] Motte L, Billoudet F, Lacaze E, Douin J and Pileni M P 2001 *J. Phys. Chem.* B **101** 138–44
[9] Lin X M, Jaeger H M and Sorensen C M 2001 *J. Phys. Chem.* B **105** 3353–7
[10] Kiely C J, Fink J, Brust M, Bethell D and Schiffrin D J 1998 *Nature* **396** 444–6
[11] Ahmed S and Ryan K M 2007 *Nano Lett.* **7** 2480–5
[12] Konstantatos G, Howard I, Fischer A, Hoogland S, Clifford J, Klem E, Levina L and Sargent E H 2006 *Nature* **442** 180–3
[13] Ross C A 2001 *Annu. Rev. Mater. Res.* **31** 203–35
[14] Lai1 S L, Guo J Y, Petrova V, Ramanath G and Allen L H 1996 *Phys. Rev. Lett.* **77** 99–102
[15] Badia A, Singh S, Demers L, Cuccia L, Brown G R and Lennox R B 1996 *Chem.—Eur. J.* **2** 359–63
[16] Luedtke W D and Landman U 1996 *J. Phys. Chem.* **100** 13323–9
[17] Chaki N K and Vijayamohanan K P 2005 *J. Phys. Chem.* B **109** 2552–8
[18] Korgel B A 2001 *Phys. Rev. Lett.* **86** 127–30
[19] Sandhyarani N, Antony M P, Selvam G P and Pradeep T 2000 *J. Chem. Phys.* **113** 9794–803
[20] Constantinides M G, Jaeger H M, Li X, Wang J and Lin X M 2007 *Z. Kristallogr.* **222** 595–600
[21] Lin X M, Sorensen C M and Klabunde K J 2000 *J. Nanopart. Res.* **2** 157–64
[22] Prasad B L V, Stoeva S I, Sorensen C M and Klabunde K J 2002 *Langmuir* **18** 7515–20
[23] Abécassis B, Testard F and Spalla O 2008 *Phys. Rev. Lett.* **100** 115504–7

[24] Murray C B, Sun S, Gaschler W, Doyle H, Betley T A and Kagan C R 2001 *IBM J. Res. Dev.* **45** 47–55
[25] Rabani E, Reichman D R, Geissler P L and Brus L E 2003 *Nature* **426** 271–4
[26] Moriaty P, Talyor M D R and Brust M 2002 *Phys. Rev. Lett.* **89** 248303–6
[27] Schultz D G, Lin X M, Li D, Gebhardt J, Meron M, Viccaro P J and Lin B 2006 *J. Phys. Chem.* B **110** 24522–9
[28] Narayanan S, Wang J and Lin X M 2004 *Phys. Rev. Lett.* **93** 135503–6
[29] Bigioni T P, Lin X M, Nguyen T T, Corwin E I, Witten T A and Jaeger H M 2006 *Nat. Mater.* **5** 265–70
[30] Lin X M, Parthasarathy R and Jaeger H M 2004 *Dekker Encyclopedia of Nanoscience and Nanotechnology* (New York: Dekker) pp 2245–58
[31] Fenter P, Eisenberger P and Liang K S 1993 *Phys. Rev. Lett.* **70** 2447–50
[32] Black C T, Murray C B, Sandstrom R L and Sun S 2000 *Science* **290** 1131–4
[33] Guo Q, Sun X and Palmer R E 2005 *Phys. Rev.* B **71** 035406